A Spatiotemporal White Noise Analysis of Photoreceptor Responses to UV and Green Light in the Dragonfly Median Ocellus

Joshua van Kleef, Andrew Charles James, and Gert Stange

Centre for Visual Sciences, Research School of Biological Sciences, Australian National University, Canberra, ACT 2601, Australia

Adult dragonflies augment their compound eyes with three simple eyes known as the dorsal ocelli. While the ocellar system is known to mediate stabilizing head reflexes during flight, the ability of the ocellar retina to dynamically resolve the environment is unknown. For the first time, we directly measured the angular sensitivities of the photoreceptors of the dragonfly median (middle) ocellus. We performed a second-order Wiener Kernel analysis of intracellular recordings of light-adapted photoreceptors. These were stimulated with one-dimensional horizontal or vertical patterns of concurrent UV and green light with different contrast levels and at different ambient temperatures. The photoreceptors were found to have anisotropic receptive fields with vertical and horizontal acceptance angles of 15° and 28°, respectively. The first-order (linear) temporal kernels contained significant undershoots whose amplitudes are invariant under changes in the contrast of the stimulus but significantly reduced at higher temperatures. The second-order kernels showed evidence of two distinct nonlinear components: a fast acting self-facilitation, which is dominant in the UV, followed by delayed self- and cross-inhibition of UV and green light responses. No facilitatory interactions between the UV and green light were found, indicating that facilitation of the green and UV responses occurs in isolated compartments. Inhibition between UV and green stimuli was present, indicating that inhibition occurs at a common point in the UV and green response pathways. We present a nonlinear cascade model (NLN) with initial stages consisting of separate UV and green pathways. Each pathway contains a fast facilitating nonlinearity coupled to a linear response. The linear response is described by an extended log-normal model, accounting for the phasic component. The final nonlinearity is composed of self-inhibition in the UV and green pathways and inhibition between these pathways. The model can largely predict the response of the photoreceptors to UV and green light.

The Journal of General Physiology

INTRODUCTION

The visual system of winged insects typically consists of two distinct subsystems. The paired compound eyes and their associated neuronal circuitry are functionally analogous to the visual system of vertebrates, forming well-resolved images and applying complex processing such as movement detection and object recognition. The dorsal ocelli are less prominent simple-lens eyes, often occurring as a triplet.

The reasons for the presence of a supplementary set of eyes are not well understood, but it is reasonable to expect that the ocelli complement rather than duplicate the compound eyes. The ocellar system is capable of mediating a rapid response because the number of synapses between receptors and descending neurons is smaller than in the compound eyes. The ocellar system has also developed receptor neurons with distinctive peak spectral sensitivities in the UV and green ranges (Ruck, 1965) and is therefore capable of processing color information. However, it is unclear whether these different spectral pathways are used concurrently or separately during the different light levels afforded to the dragonfly at daylight or dusk (Chappell and DeVoe, 1975; Klingman and Chappell, 1978).

Also, the ocelli appear to have evolved to have poor spatial resolution compared with the compound eyes (Wilson, 1978), detecting overall illumination rather than the detection of details. The optics of ocellar systems have been consistently found to be underfocused, the receptor array is irregular, and there is a large amount of convergence from receptors to second-order neurons (Warrant and McIntyre, 1993; Mizunami, 1995).

The notion that ocelli lack spatial resolution has recently been challenged by Stange et al. (2002), who concluded that the median ocellus of the dragonfly *Hemicordulia tau* is capable of image resolution. This conclusion was based on anatomical measurements, showing that the lens is unusually thick and that its vertical curvature is sufficiently strong to form a focused image on the retinal receptors. Ophthalmoscopy also showed that an incident beam of parallel light evokes tapetal reflections that originate from a small area. Such measurements can only be indicative of a potential for spatial resolution. There is currently no direct measurement of the angular sensitivities of the median ocellar receptors.

Correspondence to Gert Stange: gert.stange@anu.edu.au

Abbreviations used in this paper: MSE, mean square error; MSPE, mean square prediction error; NLN, nonlinear cascade model.

The temporal responses of these cells to relatively long (≥200 ms) high contrast square impulses have previously been measured (Chappell and Dowling, 1972; Dowling and Chappell, 1972; Simmons, 1982). However, their linear responses or responses to more ecologically realistic temporal sequences are not known as they are for other invertebrate receptors (Wong et al., 1980; Payne and Howard, 1981; Howard et al., 1984; French et al., 1993; Anderson and Laughlin, 2000; Juusola and Hardie, 2001a,b; Juusola and de Polavieja, 2003).

The temperature sensitivity of the temporal responses is also of particular interest since flying dragonflies actively thermoregulate their heads to around 10°C above the corresponding thoracic temperature (May, 1995). It is therefore likely that the ocellar receptor speed is increased at increased temperatures as has been demonstrated in receptor neurons of other invertebrates (French and Järvilehto, 1978; Tatler et al., 2000) and that their ability to encode the light signal is enhanced (Juusola and Hardie, 2001b).

In this paper we used a one-dimensional array of pairs of individually controllable UV and green light emitting diodes (LEDs) to concurrently stimulate the median ocellar receptors. In vivo intracellular recordings of the resulting membrane potential dynamics were analyzed using system identification techniques with estimation by multiple linear regression (James and Osorio, 1996; James, 2003; James et al., 2005). This allows the efficient and relatively assumption-free estimation of the spatial receptive fields and temporal response characteristics of the receptor neurons (Marmarelis and McCann, 1973; Sakai et al., 1988). The technique provides significant quantitative advantages over the methods that have previously been used to determine the receptor response characteristics in the dragonfly median ocellus (Ruck, 1961; Chappell and DeVoe, 1975; Simmons, 1982); for example, it can be used to detect nonlinear receptor responses (French et al., 1993).

We have made a quantitative analysis of the dynamic response properties of light-adapted receptors exposed to pseudorandom UV and green contrasts steps from −0.82 to 0.82. These conditions are designed to mimic those found by flying dragonflies in their natural environment. We estimated first- and second-order Wiener kernels for the light-adapted receptor responses. Temporal modulation of the linear response, coupling of the UV and green pathways, and spatial coupling between light signals from different angles are also investigated. The kernels and a parametric model are fitted to experiments performed at different ambient temperatures and contrast levels. The results are discussed in terms of the functionality of the ocellus and the underlying mechanisms responsible for receptor response.

MATERIALS AND METHODS

Animal Preparation

Single electrode recordings were made from adults of *Hemicordulia tau* (Odonata, Anisoptera, Corduliidae) that were either netted locally or reared from nymphs in the laboratory. Once obtained, animals were kept at 4°C in the dark and used within 3 d. Prior to recordings, the animals were allowed to warm up to room temperature (21–23°C) for at least 30 min. During that period, the dorsal side of the animal was fixed to a wax-covered rod of 6 mm diameter (Fig. 1 A) by first waxing its wings to the rod and then wrapping insulation tape around the thorax such that the legs were immobilized. Care was taken to allow free movement of the abdomen to maintain ventilation. The neck was slipped into an indentation in a yoke, mounted perpendicular to the end of the rod, and the hemisphere-shaped head was waxed to the yoke by its caudal rim. As the plane formed by the caudal rim is perpendicular to the longitudinal axis; this assures that the longitudinal axis is parallel to the axis of the rod, allowing precise alignment relative to the visual stimulus.

Exoskeleton and connective tissue that form part of the frons, below the ocelli, were removed, exposing the orange-pigmented capsule surrounding the retina. We further removed the esophagus and mandibles together with their associated musculature in order to reduce movement during the experiment.

Intracellular Recordings

Recording electrodes were pulled by a Flaming/Brown Micropipette puller (model P-87, Sutter Instrument Co.) and had impedances of 20–150 MΩ. A ground electrode made of chlorinated silver wire was placed firmly against an air sac adjoining the ocellus. The recording electrode was connected to a preamplifier (model 5A, Getting Instruments). The thick membrane surrounding the retina was penetrated with the recording electrode and the electrode was advanced into the retina until a small hyperpolarizing electroretinogram was detected, and was further advanced, applying a combination of manual tapping and "buzzing" the preamplifier. The electrode was considered to be intracellular when there was both a change in the light response from hyperpolarizing to depolarizing and a drop in voltage of 30 mV or more.

Recordings were made from cells that had a peak response of >5 mV to the test stimulus (see Fig. 1 B). The range of peak responses to the test stimulus was 5–20 mV, consistent with previous recordings from the ocellar receptor cells of dragonflies stimulated with large steps in contrast (Chappell and Dowling, 1972; Chappell and DeVoe, 1975; Simmons, 1982). This range of values can be attributed to the variability of response within different spatial locations of single cells (see Stone and Chappell, 1981).

In total, 58 cells were recorded from. These included 5 cells used for the temperature experiments, which were shown only stimulus type II (see below), 38 cells that were presented both stimulus types (I and II, see below), and 15 cells that were shown only one of the stimuli types because the cell was lost before a full set of measurements could be made. Cells were held on average for 12 min (range 5–90 min). An example of a recorded response to the pseudorandom stimulus type II and the difference between two repeats is shown in Fig. 1 C. The power spectrum of this response is shown in Fig. 1 D. Tissue was superfused with saline (NaCl 7.5 g/liter, KCl 0.1 g/liter, $CaCl_2$ 0.2 g/liter, $NaHCO_3$ 0.2 g/liter) throughout the experiment, maintaining a thin meniscus over the retina. The electrical signal was displayed on an oscilloscope and was recorded digitally, at a sampling rate of 5 kHz, on a PC using a 14-bit analogue to digital converter. Recorded data was later decimated (MATLAB) to reduce the effective sampling rate to the display refresh rate (625 Hz).

LED Display

The display consists of 16 pairs of green and UV LEDs (Roithner Lasertechnik B5-433-B525, peak emission at λ_{max} = 528 nm, full width at half maximum 30 nm, and Roithner Lasertechnik 380D15, peak emission at λ_{max} = 383 nm, full width at half maximum 15 nm, respectively) arranged at 5° intervals on the circumference of a circle. The dragonfly ocellus is positioned at the center of this circle (Fig. 1 A). The arrangement is attached to a cardan arm, allowing manual rotation perpendicular to the optical axes of the LEDs. This allows the display to be used as either a vertical one-dimensional display at multiple azimuths, or as a horizontal one-dimensional display at multiple elevations. The LEDs are driven by individual voltage-to-current converting driver amplifiers whose gains were set individually to match light outputs to within 5%, using either a UV-sensitive photodiode (Electro Optical Components, EPD-365-0/2.5) or a green-sensitive one (Centronic, series 15-5T) as detectors. After calibration, each of the UV LEDs produced a maximum flux of $\sim 1.2 \times 10^{14}$ photons $cm^{-2}\ s^{-1}$ at λ = 383 nm and each green one produced a maximum flux of $\sim 0.9 \times 10^{14}$ photons $cm^{-2}\ s^{-1}$ at λ = 528 nm, at the position of the ocellus.

Each driver amplifier is independently controlled via a 32-channel D/A converter with 14-bit resolution (Analogue Devices AD5532HS). The converter features a digital sample-and-hold on each channel so that pixels are only refreshed if they have changed value. The converter is driven via a microcontroller (Isopod, NewMicros Inc.) that, in turn, communicates with the PC via a parallel port. Data from the PC are converted by the microcontroller into the serial format required by the D/A converter. The display was refreshed at a rate of 625 Hz. The PC is run on the Linux operating system (Debian), with a real-time module (RTAI) for synchronous data acquisition and control, interfaced with MATLAB for higher-level functions.

Stimulus

We generated pseudorandom sequences using MATLAB's random number generator. Two types of stimulus were produced. In stimulus type I all 32 LEDs were driven by independent sequences. Stimulus type II consisted of two independent sequences, one driving all UV LEDs simultaneously and one driving all green LEDs simultaneously. In both cases the time sequences consisted of 12,512 frames. Each channel was sampled at 14-bit resolution with values uniformly distributed between 10% and 100% of maximum LED intensity. Mean intensity was thus 55% of maximum, and the contrast of values relative to the mean was uniformly distributed in the range $\pm 45/55$, that is, ± 0.82. The variance of stimulus contrast for this uniform distribution is then $0.82^2/3 = 0.22$, and standard deviation is 0.47, or $\sim$50%, with values taken to be independent and identically distributed, subject to the quality of the random number generator. An example stimulus is shown in Fig. 1 C and its power spectrum is shown in Fig. 1 D. Sequences were displayed in a repeated loop in synchrony with the data acquisition.

Temperature Experiments

Using the display in the vertical orientation, we repeated the stimulus type II experiment at elevated ambient temperatures in order to determine the effect this has on the cellular response. Heat for these experiments was provided via an air current from a small fan heater and temperature measurements were made $\sim$20–30 mm from the head of the animal, using a thermocouple. The time taken for receptors to reach thermal equilibrium with the air was experimentally determined to be 15 min, as further exposure did not increase the speed of the cellular response. After making an initial recording at room temperature the heater was turned on and 15 min allowed to elapse before further recordings were made at temperatures 7–10°C higher than the original recording. Subsequently the ambient temperature was returned to its original value and 15 min allowed to elapse before further recordings made. Cells were only considered for analysis if the time to peak of the linear response had returned to within 20% of its original value.

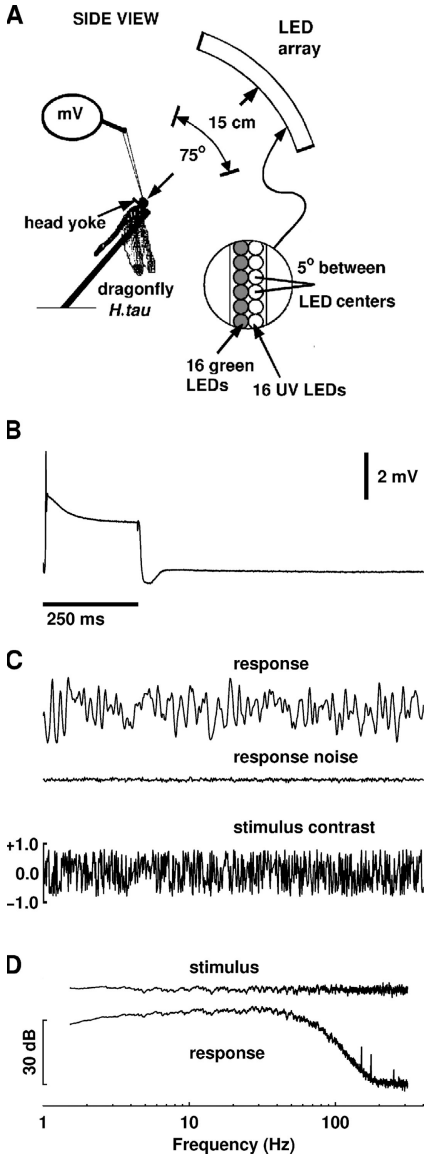

Figure 1. (A) Schematic diagram of the experimental set-up. Dragonflies were exposed to 20 s pseudorandom sequences displayed on 16 UV and 16 green LEDs, refreshed at 625 Hz. The display, shown in the vertical position, was also positioned horizontally. Changes in membrane potential (mV) were recorded intracellularly from an electrode inserted from the ventral surface. (B) Receptor response to the 250-ms test stimulus of UV and green. The response shown is an average of eight repeats. (C) The top signal shows the response of the same receptor cell as in B to the white noise stimulus type II. The noise in this response, calculated as the difference between two experimental repeats is shown below as well as the UV stimulus that produced the response (green not shown). (D) Power spectra of the stimulus and response shown in C plotted on an arbitrary (dB) scale.

The effect of temperature increases on the parameters was gauged by the Q_{10} ratio defined as the fractional increase per 10°C (Tatler et al., 2000).

Kernel Analysis

Our analysis uses a model similar to other Wiener kernel analyses of the insect visual system (Lee and Schetzen, 1965, Marmarelis and McCann, 1973; McCann, 1974; James and Osorio, 1996; Juusola and French, 1997) but with kernels estimated by multiple linear regression (James, 2003; James et al., 2005). The contrast level at each point of elevation or azimuth is defined as $c = (I - I_0)/I_0$, where I is the intensity level at that point and I_0 is its mean temporal intensity. Contrast is dimensionless, but for clarity it is represented as having units C. Note that stimulus consists of independent identically distributed values with expected value zero and variance $V_c = 0.22$. We assume that the receptor response y (mV) at sample steps t, running from 0, . . . ,12511, is dependent on the UV contrast levels $c_u(\theta, t\text{-}\tau)$ and green contrast levels $c_g(\theta, t)$ at either azimuth or elevation θ, for $\theta = \theta_1, \theta_2, \ldots, \theta_{16}$, and at preceding time steps $t\text{-}\tau$, and that the relationship is described by the discrete Wiener series to second order, plus hum and noise terms:

$$y(t) = f_0 + f_u(t) + f_g(t) + f_{uu}(t) + f_{ug}(t) + f_{gg}(t) + f_{hum}(t) + e(t) \quad (1)$$

The term f_0 produces a constant offset. The term $f_u(t)$, models the first-order responses due to stimulation by UV contrast modulation, given by the convolution:

$$f_u(t) = \sum_{\tau_1 = 0}^{\tau_m} \sum_{\theta = \theta_1}^{\theta_{16}} h_u(\theta,\tau_1) \cdot c_u(\theta, t - \tau_1), \quad (2)$$

which sums values of the stimulus c_u over preceding time steps up to memory length τ_m and over angle, weighted by the first-order kernel $h_u(\theta, \tau_1)$. The term f_g is the corresponding component for first-order response to green contrast, involving kernel $h_g(\theta, \tau_1)$.

The second-order (quadratic) term $f_{uu}(t)$ is given by

$$f_{uu}(t) = \sum_{\tau_1 = 0}^{\tau_m} \sum_{\tau_2 = 0}^{\tau_m} \sum_{\theta = \theta_1}^{\theta_{16}} h_{uu}(\theta,\tau_1,\tau_2) \cdot \quad (3)$$

$$[c_u(\theta, t - \tau_1) \cdot c_u(\theta, t - \tau_2) - V_c \cdot \delta(\tau_2 - \tau_1)],$$

which sums product terms in the stimulus c_u over pairs of preceding time steps up to memory length τ_m and over angle, weighted by the second-order kernel $h_{uu}(\theta, \tau_1, \tau_2)$.

Values of the stimulus sequence c_u are independent zero-mean random variables. The term $-V_c \cdot \delta(\tau_2 - \tau_1)$ subtracts the variance of the stimulus, $V_c = 0.22$ at points in the summation where $\tau_1 = \tau_2$ and is otherwise zero. This ensures that the expected value of the term $f_{uu}(t)$ is zero for our stimulus input statistics, hence that the output is in expectation uncorrelated with the zero-order term f_0. It is this property that makes the series a Wiener series relative to these input statistics. This formulation makes the Wiener model a sum of dual pairings between the kernels, and the members of a polynomial orthogonal basis in the input values, as defined by Yasui (1979).

The terms f_{gg} and f_{ug} give the corresponding components for second-order response to green contrast and the interaction component for UV and green input, although the interaction component f_{ug} does not require the correction term.

The term $f_{hum}(t)$ fits a component due to 50 Hz mains hum, which is modeled as a series of the first six terms in a harmonic sine and cosine series with a fundamental frequency of 50 Hz. The contribution of intrinsic and other experimental noise to the recorded signal is represented by e(t).

The receptor model considered here is therefore defined by its Wiener kernels h_u, h_g, h_{uu}, h_{gg}, and h_{ug}. For each experimental run, the raw experimental data were preprocessed by removing low frequency drift observed in the signals over the 20-s recording period. Low frequency drift was removed by fitting a fourth-order polynomial to the raw data and removing it from the signal. The residual results were fitted to the model described by Eq. 1 using multiple linear regression (James, 2003; James et al., 2005), which produces the estimates of the kernels minimizing the sum of squares of the residuals, e(t). Simulations with predefined systems and multiple realizations of stimulus sequences and experimental noise indicate that the least-squares estimates have expected value equal to the true Wiener kernels of the system, and that this is true even in the presence of higher-order nonlinearity, which is not fitted in the model (unpublished data). Detrended and hum corrected data for each experimental run (y_d) were obtained from the preprocessed data by removing the fitted components $f_0 + f_{hum}$.

Using multiple runs (2–9) we used a "leave one out" cross-validation method to calculate the prediction error. In this method, a single detrended dataset is compared with the values predicted by a model whose parameters are obtained from the mean of the parameters fitted to each of the other datasets. The mean square prediction error (%MSPE) is reported as a percentage of the signal power of the detrended data, defined as (Juusola et al., 2003):

$$\%\text{MSPE} = 100 \cdot \frac{\overline{(f_m - f_d)^2}}{\overline{(y_d - \bar{y}_d)^2}}, \quad (4)$$

where the bar represents the temporal mean, f_m is the predicted value, and y_d is the detrended hum-corrected signal. The reported %MSPE is actually the mean of the %MSPE calculated for different experimental runs.

To ascertain an optimal value of τ_m (the memory of the system), it was increased until the %MSPE for the corresponding kernels either increased or if it decreased by <0.01%. The same process was used to ascertain the validity of adding nonlinear terms to the model.

Space–Time Separability

Separable models for the kernel h_u are those written as the outer product of a spatial profile (ρ_u) and temporal waveform (ψ_u) of the kernel such that the value of h_u at time τ and angle θ is given by $h_u(\tau, \theta) = \rho_u(\theta)\psi_u(\tau)$, with similar expressions for the green kernel $h_g(\tau, \theta)$. Note that θ is the angle of elevation or azimuth depending on whether the display was mounted vertically or horizontally. Estimates of the spatial profiles and temporal waveforms were obtained using singular value decomposition (SVD), which produces the space–time decomposition with least-square deviation from the two-dimensional kernel. The absolute magnitude of the kernel was determined by the temporal component with the spatial component set to have a maximum value of unity.

Kernels were deemed to be separable if the kernel reconstructed from these components produced a percentage mean squared error of <10% of the original kernel. The percentage mean square error (%MSE) of the reconstructed kernel was calculated as a percentage of the original kernel power in a similar fashion to Eq. 4

$$\%\text{MSE} = 100 \times \overline{(h_u - \rho_u \Psi_u)^2} / \overline{(h_u - \bar{h}_u)^2},$$

with the mean taken over space and time, and similarly for green.

Linear Parametric Model

An extended log-normal function (Payne and Howard, 1981) was fitted to the first-order (linear) kernels in order to characterize their temporal profiles. The log-normal model for the UV kernel is defined as:

$$G_u(t_n) = v_u \exp(-\{\log(t_n/t_u^p)\}^2/2\sigma_u^2), \quad (5)$$

where t_u^p is the time to peak, σ_u determine the width, and v_u is the amplitude (units $mV(C \cdot ms)^{-1}$) of the UV response. By adding a term proportional to the derivative of the G_u we extended Eq. 5 so that the extended model H_u becomes:

$$H_u(t_n) = G_u(t_n) + \tau_u^d \frac{dG_u(t_n)}{dt_n}, \quad (6)$$

where τ_u^d (units ms) determines the relative proportion of the derivative added to the log-normal model. Equivalent expressions were used to describe the green response H_g in terms of the equivalent parameters t_g^p, σ_g, v_g, and τ_g^d.

NLN Sandwich Model

We fitted a nonlinear cascade model (NLN) to the data where the first stage of the model consists of separate positive static nonlinearities for the UV and green response. The resulting outputs for the static UV $p_u(t)$ and green $p_g(t)$ nonlinearities are given by $p_u(t) = c_u(t) + a_1 c_u(t)^2$ and $p_g(t) = c_g(t) + a_2 c_g(t)^2$ where a_1 and a_2 are positive constants.

The middle linear filters for the UV and green pathways are obtained from fitting the extended log-normal function (Eq. 6 and the green equivalent) to the UV and the green first-order kernels. The outputs from the second stage of the UV pathway are given by the discrete convolution:

$$q_u(t) = \sum_{\tau=0}^{\tau_m} H_u(\tau) \cdot p_u(t-\tau) d\tau, \quad (7)$$

and a similar expression describes the output from the second stage of the green pathway, $q_g(t)$.

The third stage consists of a sum of the second stage outputs $q_u(t)$ and $q_g(t)$ together with three delayed and inhibitory nonlinearities. These nonlinearities account for the inhibition of the UV and green output from the second stage of the model. The final output $r(t)$ of the model is given by:

$$r(t) = q_u(t) + q_g(t) - c_1 q_u(t-\tau_i)^2 - c_2 q_u(t-\tau_i) q_g(t-\tau_i) - c_3 q_g(t-\tau_i)^2, \quad (8)$$

where c_1, c_2, and c_3 are positive constants and τ_i is the time delay of the inhibition.

Simulated annealing (Press et al., 1993) was employed to search for the parameters of the nonlinear model (Eq. 8) that minimized the least squares difference between the model response (r) and y_d, the detrended experimental recording. This was performed for each repeat and, using the same cross-validation technique used for the Wiener kernels, the %MSPE for the NLN model was calculated.

Frequency Response

The power spectra of the detrended hum-corrected signals, and signals reconstructed from the convolution of the kernels with the input stimuli, were obtained by taking an 8192-point fast fourier transform of their respective autocorrelation functions. These calculations were performed in MATLAB using its xcorr and fft functions. The resulting power spectra were smoothed by taking an 80-point moving average.

RESULTS

Responses to Spatially Modulated Stimuli (Stimulus Type I)

Using the spatiotemporal pseudorandom stimulus, where each UV and green LED was independently modulated, we were able to obtain first-order space-time kernels for the UV and green response. We also fitted further models with second-order terms representing spatial interactions between cells, coupling between UV and green pathways and nonlinear temporal modulation of the response, but found that the inclusion of any of these terms did not reduce the mean %MSPE for any cells. Thus, for stimulus type I patterns, the receptors are acting linearly and we find no evidence for spatial interactions between cells.

According to the cross-validation procedure (methods), under stimulus type I conditions the memory (τ_m) that produced optimal %MSPEs was 48 ms. Although some cells benefited from fits to kernels with τ_m up to 64 ms, the reduction in %MSPE for these cells was $<0.01\%$. We therefore estimated all kernels for stimulus type I using $\tau_m = 48$ ms.

The linear Wiener kernel models gave an average %MSPE of 9.7% ($n = 18$ cells) in the vertical plane and 7.8% ($n = 25$ cells) in the horizontal plane. The average root mean square (RMS) values of the detrended signal (y_d) and kernel fit were respectively: 0.30 mV (SD = 0.11) and 0.28 mV (SD = 0.10), for the vertical plane, and 0.22 mV (SD = 0.10) and 0.19 mV (SD = 0.06), for the horizontal plane.

UV space–time kernels were well described by the kernels reconstructed from their spatial and temporal components obtained through singular value decomposition. The percentage mean square error of the reconstructed kernels, as a percentage of the original kernel power, was in the range 0.1–5.0%. For green kernels, we found that 15 out of 43 cells had green space–time kernels that were not separable (%MSE range of 11.1–56.3%). The difference between the kernel and the outer product of the spatial and temporal components could be attributed to recording artifacts and the amount of noise in the kernel estimate.

Angular Sensitivities (ρ_u and ρ_g)

Fig. 2 shows examples of the UV and green spatial components of first-order kernels for three receptor neurons, in the dimension of elevation. The LED array was mounted vertically on a cardan arm that allowed manual adjustment in azimuth. The recordings were obtained after positioning it at the azimuth of maximum sensitivity to brief flashes of light from all LEDs in the array. We notice that those particular neurons had their maximum responses at elevations of 20° (Fig. 2, A and C) and at 2.5° (Fig. 2 B) above the horizon; on either side of this maximum, the responses fall off rapidly.

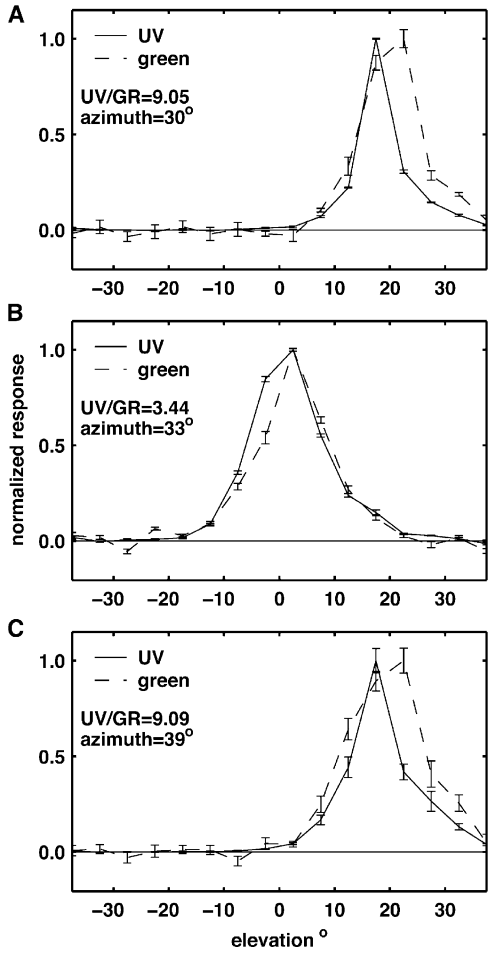

Figure 2. Normalized angular sensitivities in elevation to UV (ρ_u) and green (ρ_g) light are shown for three cells A, B, and C. These were obtained by performing a singular value decomposition of the first-order spatiotemporal kernels estimated for these cells. The UV to green ratio, at peak response, is given for each cell (UV/GR), as well as the azimuthal position of the vertically mounted display. Error bars indicate SEM.

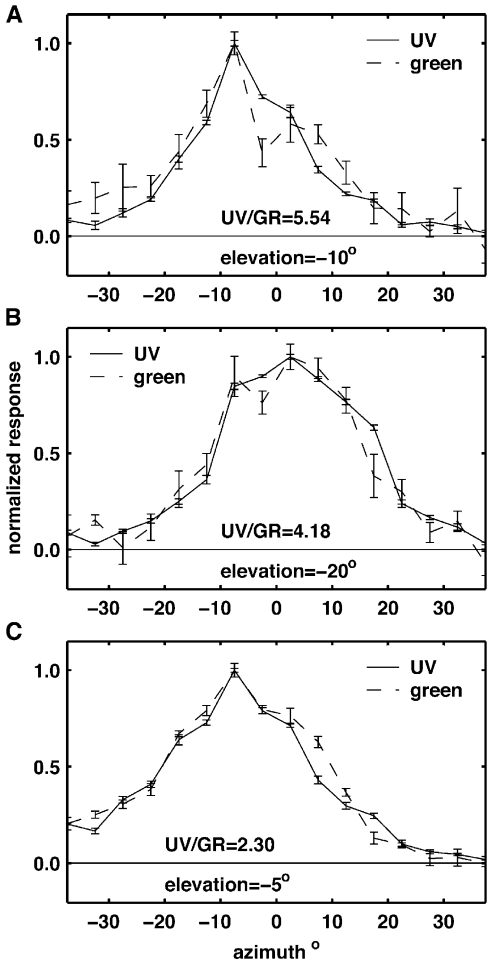

Figure 3. Angular sensitivities in azimuth to UV (ρ_u) and green (ρ_g) light are shown for three cells (A, B, and C). Details are the same as in Fig. 2 but with the elevation of the horizontally mounted display given for each cell.

Fig. 3 shows analogous measurements in azimuth, obtained independently, on different animals. Here, the array was mounted horizontally, allowing adjustment in elevation. It is apparent that the responses extend over a wider range of angles.

Elevation measurements were repeated for a total of 16 receptor neurons. The mean value of the acceptance angles, $\Delta\rho$ (defined as the response's full width at half maximum, FWHM), is 14.7°, with a standard deviation of 4.3°. To summarize results, angular sensitivities were mapped against locations in azimuth, as shown in Fig. 4 A. The dashed ellipse represents the outline of the total field of view of the ocellus, of 120° × 60° as determined in eyeshine measurements by Stange et al. (2002).

A corresponding dataset was obtained for azimuth measurements. A total of 21 neurons were tested; the mean acceptance angle was 27.6°, with a standard deviation of 4.6°. To summarize results, angular sensitivities were mapped against locations in elevation, as shown in Fig. 4 B.

All responses occurred to the left of the vertical midline, consistent with the fact that all recordings were made from the right retina. There is a bias toward the upper half of the receptive field, which we attribute to bias in the recording procedure: the electrode was always inserted into the retina from its ventral side, with the consequence that upwards-looking receptor neurons were encountered first. We also noticed that 29 of the 37 receptive fields are within ±15° of midline. We attribute this to the fact that the receptor neurons at the center of the retina are much larger than those at the periphery (Stange et al., 2002), with the consequence that recordings from those neurons are more likely.

As there is no evidence for any systematic variation of angular sensitivities with position on the retina, we in-

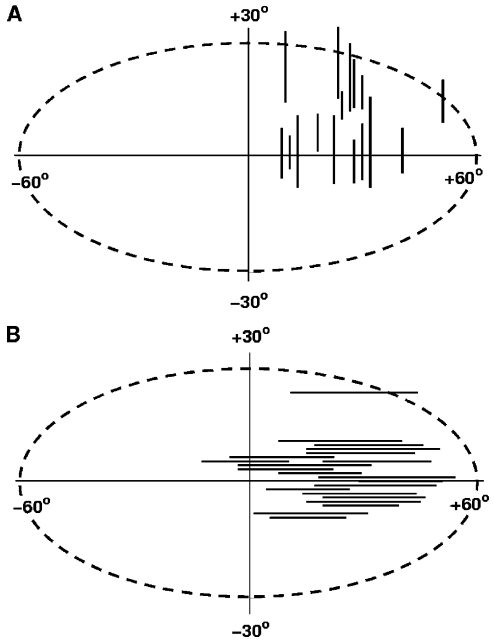

Figure 4. (A) Elevation angular sensitivities of 16 receptor neurons and (B) azimuthal angular sensitivities of 25 receptor neurons. Lines represent the spans for which responses were >50%. The dashed ellipses (width 120°, height 60°) represent the total field of view of the ocellus, as determined by optical measurements.

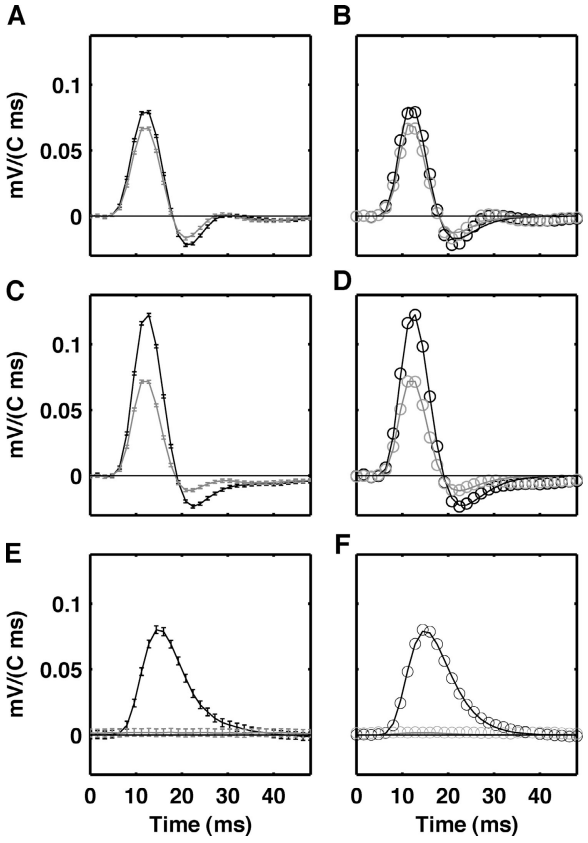

Figure 5. Time components of UV (ψ_u) and green (ψ_g) first-order kernels (A, C, and E) and modified log-normal fits to these functions for the same three cells (B, D, and F). The black and gray lines indicate UV and green response, respectively. Error bars indicating the SEM in the time component of the first-order kernels are shown in (A, C, and E). The circles in B, D, and F represent the kernel values fitted. Parameter values obtained from fits to Eq. 6 are: B(a) UV $v_u = 0.034$ mV(C·ms)$^{-1}$, $t_u^p = 15.7$ ms, $\sigma_u = 0.281$, $\tau_u^d = 10.5$ ms, and green $v_g = 0.032$ mV(C·ms)$^{-1}$, $t_g^p = 15.4$ ms, $\sigma_g = 0.272$, $\tau_g^d = 8.8$ ms; B(b) UV $v_u = 0.051$ mV(C·ms)$^{-1}$, $t_u^p = 16.4$ ms $\sigma_u = 0.291$, $\tau_u^d = 10.9$ ms, and green $v_g = 0.034$ mV(C·ms)$^{-1}$, $t_g^p = 15.7$ ms, $\sigma_g = 0.283$, $\tau_g^d = 8.8$ ms; B(c) UV $v_u = 0.068$ mV(C·ms)$^{-1}$, $t_u^p = 17.7$ ms, $\sigma_u = 0.300$, $\tau_u^d = 2.9$ ms, and green $v_g = 0.002$ mV(C·ms)$^{-1}$, $t_g^p = 14.7$ ms, $\sigma_g = 0.396$, $\tau_g^d = 1.1$ ms.

fer that a typical receptor neuron has a FWHM field of view that is elliptical, covering 14.7° in elevation and 27.6° in azimuth. The total field of view of the median ocellus is 60 × 120°, as inferred from eyeshine measurements. Therefore, that field could accommodate four independent sampling stations or pixels in azimuth and four pixels in elevation. It needs to be considered, however, that the total number of receptor neurons is ~1,500, implying spatial oversampling by a factor of 10 in each dimension. Such oversampling could, for instance, improve signal-to-noise ratio at low intensities or contrasts, or it could be relevant for fast motion detection.

Temporal Responses (ψ_u and ψ_g)

Time components of the linear response were characterized by a latency of ~5 ms followed by a depolarization that peaked at ~14 ms. Temporal responses for three cells are shown in Fig. 5 (A, C, and E). In all but two cells, the tail of the transient included a distinctive undershoot of the resting potential followed by a slow return to the equilibrium value (seen in Fig. 5, A and C, but not E).

There were no discernible differences in the shape of the linear kernels for UV and green light in each cell. The UV–green ratio, measured as the ratio of the peak values of h_g and h_u, varied widely between cells, ranging from ~0.9 to ~10.5. We also observed that the mean UV–green ratio was not significantly different for cells illuminated with the horizontal display, where it was 0.27 (SD = 0.20), from what it was for those exposed to the vertical setup, where it was 0.24 (SD = 0.18).

Parametric Modelling

Although the kernel model provides a description that is capable of predicting, on average, 87.9% of the signal power in the receptor responses it requires 32 (LEDs) × 31 (timesteps) = 992 parameters in order to achieve this accuracy. To obtain a more succinct description of the responses we attempted to fit a parametric model. The spatial profiles were kept as 16 discrete values (see Figs. 2 and 3). This was because fitted

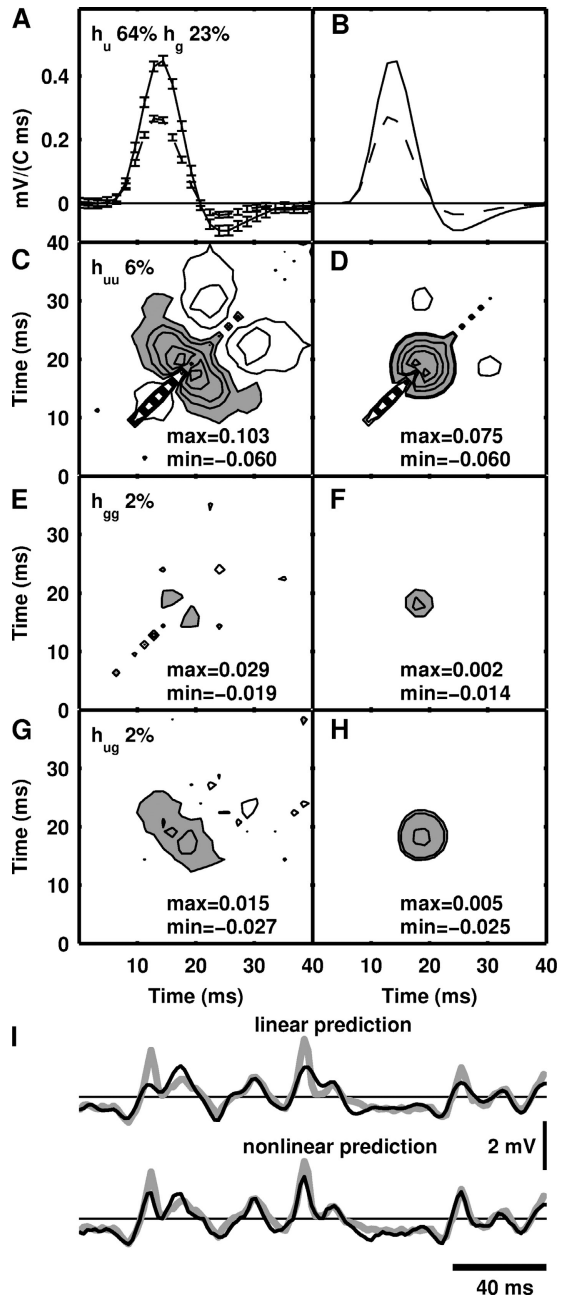

Figure 6. First-order (A and B) and second-order (C–H) temporal kernels together with the reconstructed signals of a receptor with a small nonlinear component. Kernels were estimated using multiple linear regression on the detrended data y_d (A, C, E, and G) or produced from directly fitting the NLN sandwich model described by Eqs. 6 and 7 (B, D, F, and H). Percentages show the power of the reconstructed signal of the kernels as a percentage of detrended signal power. Maximum and minimum values are given at the bottom of each figure and the negative regions of these kernels, indicating inhibition, are shaded. Contours are at 10% levels of the maximum value of the kernel in each case. (A and B) First-order kernels h_u (solid line) and h_g (dashed line) that describe the linear response of a receptor to UV and green contrasts, respectively. Error bars in A indicate the SEM. (C and D) The second-order kernels h_{uu} that account for UV light potentiating the response of the cell to UV light. (E and F) The second-order kernels h_{gg} that account for green potentiation of the green response. (G and H) The cross-kernels h_{ug} that account for the interactions between UV and green response. The equivalent kernels for A, C, E, and G were produced with linear UV parameters: $v_u = 0.193$ mV(C·ms)$^{-1}$, $t_u^p = 18.0$ ms, $\sigma_u = 0.281$, $\tau_u^d = 11.2$ ms, and linear green parameters: $v_g = 0.133$ mV(C·ms)$^{-1}$, $t_g^p = 17.5$ ms, $\sigma_g = 0.290$, and $\tau_g^d = 9.2$ ms. The nonlinear model parameters for this model are: $a_1 = 0.171$ C^{-1}, $a_2 = 0.0$ C^{-1}, $b_1 = 0.008$ mV^{-1}, $b_2 = 0.010$ mV^{-1}, $b_3 = 0.005$ mV^{-1}, $\tau_i = 4.9$ ms. I. The measured response of a receptor cell (thick gray line) is shown for an interval of 200 ms together the predicted signals (dark lines) from linear kernel alone (linear prediction) and combined linear and nonlinear kernels (nonlinear prediction).

Gaussian functions did not provide adequate parametric descriptions.

We considered two temporal models that have previously been used to describe the linear receptor response of invertebrates: the log-normal model (Payne and Howard, 1981) and the gamma function model (Wong et al., 1980). As these models describe a purely tonic response to light and our measured first-order kernels contained significant phasic components (see Fig. 5, A and C), we extended them by adding a component proportional to their time derivatives. This process was not based on an understanding of the underlying biophysical processes but nevertheless allowed us to introduce a phasic component to the original models, with the addition of only a single parameter: the constant of proportionality.

The extended models were then fitted to the temporal components of the first-order kernel estimations ($\psi_u(\tau)$ and $\psi_g(\tau)$). We found that the extended log-normal model provided a marginally better description so this model was used throughout the paper (Eq. 6). Examples of three fits to extended log-normal functions are shown in Fig. 5 (B, D, and F) alongside the first-order kernels they were fitted to (Fig. 5, A, C, and E).

The fits of Eq. 6 to the temporal profiles of UV, $\psi_u(t)$, and green, $\psi_g(t)$, response were combined with their corresponding spatial profiles ρ_u and ρ_g obtained from singular value decomposition (SVD) (see MATERIALS AND METHODS). The reconstructed spatiotemporal kernels gave mean %MSE values of 11.0% ($n = 18$) for the vertical display and 11.9% ($n = 25$) for the horizontal display. Values for the parameters obtained from these fits are given in Table II.

The mean value of the amplitude of the UV waveform v_u was found to be significantly higher for cells stimulated with the vertical setup than it was for those stimulated with the horizontal setup: 0.098 mV (C·ms)$^{-1}$ compared with 0.054 mV(C·ms)$^{-1}$, and the distribution of values obtained was wider: SD = 0.043 mV(C·ms)$^{-1}$ compared with SD = 0.022 mV(C·ms)$^{-1}$. We found that in all cells there were no significant differences between the shape of the responses to UV and green light. For this reason we report the mean values

TABLE I

Prediction Error Residuals for the First- and Second-order Kernels and Linear and Nonlinear Parametric Models (% MSPEs)

Model fitted	$f_u + f_g$	$f_u + f_g + f_{uu} + f_{ug} + f_{gg}$	Eq. 6	Eqs. 6 and 7
Stimulus Type I				
Vertical, $n = 18$				
Linear cells	9.7, $n = 18$	–	11.2, $n = 18$	–
Nonlinear cells	–	–	–	–
Horizontal, $n = 25$				
Linear cells	7.8, $n = 25$	–	12.1, $n = 25$	–
Nonlinear cells	–	–	–	–
Stimulus Type II				
Vertical, $n = 16$				
Linear cells	2.5, $n = 12$	–	14.2, $n = 12$	–
Nonlinear cells	18.0, $n = 4$	11.7, $n = 4$	19.1, $n = 4$	15.8, $n = 4$
Horizontal, $n = 32$				
Linear cells	13.5, $n = 3$	–	15.4, $n = 3$	–
Nonlinear cells	18.1, $n = 29$	12.9, $n = 29$	18.5, $n = 29$	15.7, $n = 29$
Control, $n = 5$				
Linear cells	–	–	–	–
Nonlinear cells	21.2, $n = 5$	12.7, $n = 5$	22.6, $n = 5$	13.9, $n = 5$
Hot, $n = 5$				
Linear cells	–	–	–	–
Nonlinear cells	13.0, $n = 5$	7.1, $n = 5$	13.4, $n = 5$	9.7, $n = 5$

of σ_u and σ_g, τ_u^d and τ_g^d, and t_u^p and t_g^p, concurrently (Table II). There were also no significant differences between the values of these parameter values obtained in cells stimulated with either a horizontal or vertical stimulus (see Table II).

Responses to Ganzfeld Stimuli (Stimulus Type II)

To probe the response dynamics at higher contrast levels we modulated either of the rows of 16 UV LEDs and 16 green LEDs synchronously in two separate pseudorandom sequences. The inclusion of second-order kernels h_{uu}, h_{ug}, and h_{gg} reduced the %MSPEs of 4 out of 16 cells stimulated with the display in the vertical position (see %MSPEs in Table I). These cells are classified as "nonlinear" cells. We found that a greater proportion of cells stimulated with the display in the horizontal position were found to be nonlinear (29/32). This difference was not consistent with these cells being driven further from their equilibrium into a nonlinear range as the average root mean square (RMS) values of the detrended signal and kernel fit were respectively: 0.70 mV (SD = 0.30) and 0.67 mV (SD = 0.28), for the vertical stimulus, and 0.57 mV (SD = 0.27) and 0.55 mV (SD = 0.27), for the horizontal stimulus.

Linear and Nonlinear Temporal Response

The shapes of the first-order temporal kernels obtained using stimulus type II were similar to those calculated using the stimulus type I, however the amplitudes v_u and v_g are larger (see Table II). This is attributable to

TABLE II

Estimated Parameters of the Extended Log-normal Model

	Stimulus Type I		Stimulus Type II			
Quantity, symbol, units	Vertical	Horizontal	Vertical	Horizontal	32°C–35°C	Control
Time to peak, t_u^p and t_g^p, ms	17.4	16.6	17.4	16.3	11.1	17.6
SD, n	1.6, 36	1.1, 50	0.5, 32	0.9, 64	1.0, 10	1.5, 10
Width parameter σ_u and σ_g	0.292	0.287	0.297	0.279	0.275	0.280
SD, n	0.026, 36	0.033, 50	0.012, 32	0.015, 64	0.009, 10	0.017, 10
UV amplitude, v_u, mV(C·ms)$^{-1}$	0.098	0.054	0.32	0.25	0.55	0.28
SD, n	0.043, 18	0.022, 25	0.12, 16	0.13, 32	0.30, 5	0.04, 5
Green amplitude, v_g, mV(C·ms)$^{-1}$	0.017	0.012	0.09	0.08	0.15	0.07
SD, n	0.010, 18	0.007, 25	0.04, 16	0.05, 32	0.15, 5	0.03, 5
Derivative coefficient, τ_u^d and τ_g^d, ms	12.2	11.2	11.8	9.8	6.2	12.8
SD, n	7.8, 36	1.0, 50	3.0, 32	4.7, 64	0.9, 10	3.8, 10

the fact that the kernels obtained with stimulus type II represent the response of the cell to all 16 UV or 16 green LEDs, whereas in the case of type I the kernels represent the response to the modulation of a single LED (UV or green).

Fig. 6 A and Fig. 7 A show examples of the linear kernels for UV (h_u) and green (h_g) response of cells exposed to stimulus type II. First-order UV kernels were found, on average, to account for 80.9% (SD = 5.0%, $n = 4$) of the detrended signal power when measured with the vertically mounted stimulus and 81.5% (SD = 21.5%, $n = 29$) when measured with the horizontally mounted display. First-order green kernels accounted for much less of the signal power: 8.7%, SD = 6.5%, $n = 4$ (vertically mounted display) and 8.4%, SD = 8.3%, $n = 29$ (horizontally mounted display).

The signal reconstructed from the convolution of UV contrast inputs with the second-order kernel h_{uu} contained more power as a percentage of signal power (mean = 8.3%, SD = 4.8%) than that reconstructed from the kernels that describe green–green (mean = 2.5%, SD = 2.6%) or UV–green interactions (mean = 2.8%, SD = 2.8%).

In all cells where the addition of nonlinear terms improved the fit, we found static UV facilitation of the response to UV light. Fig. 6 C and Fig. 7 C show typical UV–UV kernels demonstrating facilitation of the response, represented by a narrow ridge along the diagonal. Although early positive diagonals were seen on all UV–UV kernels and some green–green kernels they were not observed in the cross-kernels, h_{ug}, in any of the cells. If a common process did underlie nonlinear summation of UV and green responses then we would expect a positive ridge in the cross-kernel h_{ug}. Thus, separate processes within the cell must underlie the facilitation of the UV and green responses. These may be of the same biochemical nature but if this were the case they must occur in separate cells or subcellular compartments.

The maximum facilitation seen in the UV–UV kernel had a mean value 0.109 mV$(C\cdot ms)^{-2}$ (SD = 0.043 mV$(C\cdot ms)^{-2}$, $n = 32$), which was larger than that seen in the green–green and UV–green kernels that had mean values of 0.037 mV$(C\cdot ms)^{-2}$ (SD = 0.032 mV$(C\cdot ms)^{-2}$, $n = 32$) and 0.024 mV$(C\cdot ms)^{-2}$ (SD = 0.016 mV$(C\cdot ms)^{-2}$, $n = 32$), respectively.

An example of h_{gg} is shown in Fig. 6 E. Overall the self-facilitation of the green light response was smaller than it was for UV light. However, the mean value of maximal inhibition for h_{gg} (−0.051 mV $(C\cdot ms)^{-2}$, SD = 0.037 mV$(C\cdot ms)^{-2}$, $n = 32$) was closer to that of h_{uu} (−0.067 mV$(C\cdot ms)^{-2}$ (SD = 0.043 mV$(C\cdot ms)^{-2}$, $n = 32$), while the mean minimum of h_{ug} was −0.021 mV$(C\cdot ms)^{-2}$ (SD = 0.0134 mV$(C\cdot ms)^{-2}$, $n = 32$). Examples of the cross-kernel, h_{ug}, are shown in Fig. 6 G, Fig. 7 G, Fig. 8 (G and H), and Fig. 9 (G and H). Note the absence of any facilitation along the diagonal.

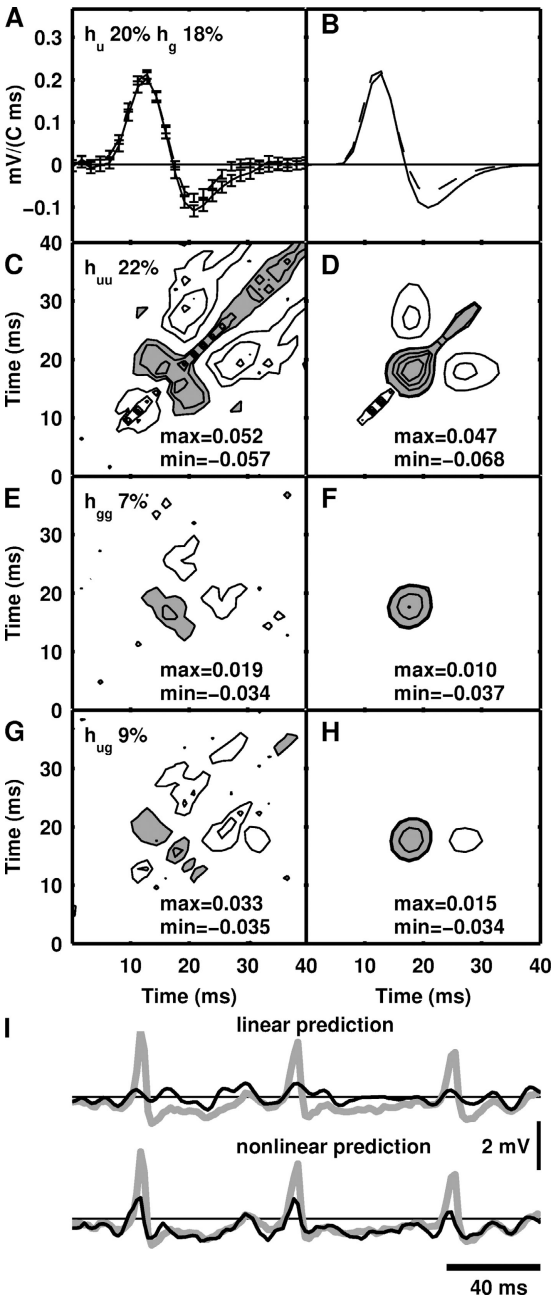

Figure 7. First-order (A and B) and second-order (C–H) temporal kernels estimated directly from the data (A, C, E, and G) or from the NLN model (B, D, F, and H) are shown for a receptor with a larger nonlinear component of response. The full and linear kernel predictions of the response are shown separately in I. Details are the same as Fig. 6, however contours are at 20% levels. The linear UV parameters used are: $v_u = 0.030$ mV$(C\cdot ms)^{-1}$, $t_u^p = 16.4$ ms, $\sigma_u = 0.259$, $\tau_u^d = 41.5$ ms, and linear green parameters are: $v_g = 0.076$ mV$(C\cdot ms)^{-1}$, $t_g^p = 15.8$ ms, $\sigma_g = 0.259$, and $\tau_g^d = 13.1$ ms. The nonlinear model parameters obtained from fit are: $a_1 = 0.226\ C^{-1}$, $a_2 = 0.042\ C^{-1}$, $b_1 = 0.037\ mV^{-1}$, $b_2 = 0.039\ mV^{-1}$, $b_3 = 0.019\ mV^{-1}$, $\tau_i = 5.5$ ms.

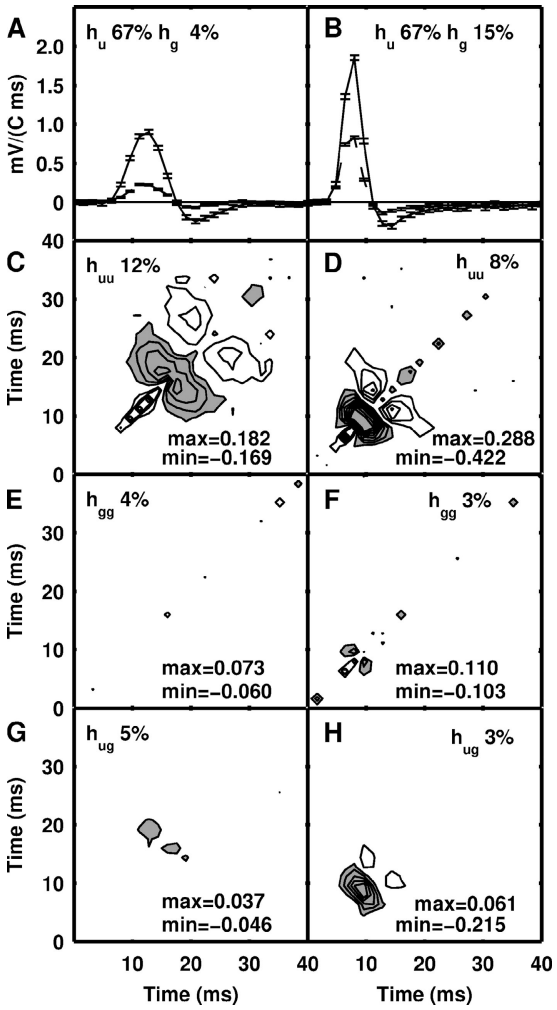

Figure 8. First-order kernels for UV (h_u), green (h_g) (A and B), together with their second-order kernels h_{uu} (C and D), h_{gg} (E and F), and h_{ug} (G and H) for a cell at 22°C (A, C, E, and G) and 33°C (B, D, F, and H). Details for both columns are the same as the left hand side of Fig. 6 (A, C, E, and G). In this cell, the relative UV to green ratio of the cell is reduced at the elevated temperature.

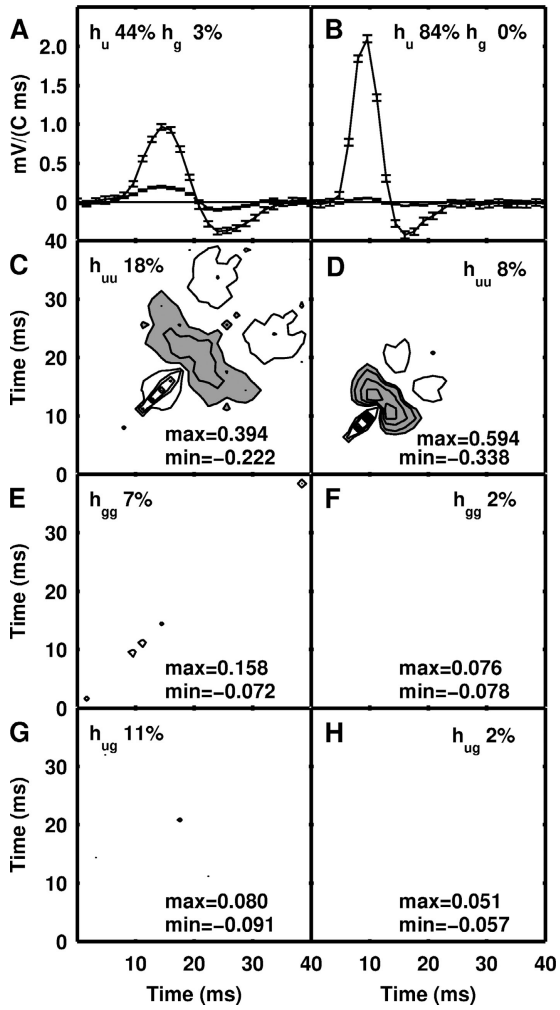

Figure 9. First-order kernels for UV (h_u), green (h_g) (A and B), together with their second-order kernels h_{uu} (C and D), h_{gg} (E and F), and h_{ug} (G and H) for a cell at 22°C (A, C, E, and G) and 32°C (B, D, F, and H). Details are the same as for Fig. 8. In this case the relative UV to green ratio of the maximal cell response is increased at the elevated temperature and the power in the nonlinear kernels is reduced.

Timing of Facilitation

In 37/38 cells the maximum self-facilitation of UV was observed along the diagonal and at a time that closely followed the peak linear UV response. The peak occurred along the diagonal in h_{uu} on average at t = 12.8 ms (SD = 2.3, n = 31). The peak UV linear response occurred, on average, 0.5 ms (SD = 0.8, n = 37) before the peak UV–UV facilitation.

The maximum self-facilitation of the green response also occurred mostly along the diagonal (36/38) cells. The green–green second-order kernels contained higher levels of noise. This reduced the number of cells whose peak green–green facilitation could be reliably comparable to their linear green response from 38 to 22. The peak green–green interaction for these cells occurred at a mean of 12.0 ms (SD = 1.3, n = 22), which was, on average 0.9 ms (SD = 1.3, n = 22) after the peak linear green response.

Timing of Inhibition

Peak facilitation occurred at the time of maximal linear response so we may have expected that similarly maximal inhibition would coincide with minimum linear response. Instead the maximal inhibition was delayed against the peak response and preceded the minimum response.

The maximal inhibition found in h_{uu} occurred off the diagonal at mean times t_1 = 16.0 ms (SD = 1.6, n = 38) and t_2 = 18.2 ms (SD = 1.6, n = 38). Although the second of these times is closer to the time of minimum UV linear response, in all cells, it was found to be signif-

TABLE III

NLN Sandwich Model Parameters

Quantity, symbol	Units	Vertical, $n = 4$	Horizontal, $n = 29$	33°C–35°C, $n = 5$	Control, $n = 5$
First nonlinearity					
UV–UV facilitation, a_1	C^{-1}	0.158	0.174	0.176	0.153
SD		0.049	0.043	0.030	0.022
Green–green facilitation, a_2	C^{-1}	0.026	0.037	0.064	0.027
SD		0.033	0.047	0.067	0.037
Second nonlinearity					
UV–UV inhibition, b_1	mV^{-1}	0.005	0.009	0.005	0.006
SD		0.001	0.009	0.002	0.001
Green–green inhibition, b_3	mV^{-1}	0.009	0.012	0.029	0.009
SD		0.006	0.014	0.053	0.008
UV–green inhibition, b_2	mV^{-1}	0.010	0.014	0.010	0.011
SD		0.007	0.013	0.003	0.004
Inhibitory delay, τ_i	ms	4.8	4.0	2.0	5.0
SD		0.2	0.8	0.9	1.3

icantly different, preceding it by a mean of 5.3 ms (SD = 2.0, $n = 38$).

Similarly, maximal inhibition in the green–green and UV–green kernels peaked after the maximum linear response but before the minimum linear response.

Parametric Modelling

The presence of the narrow ridge along the diagonal indicated that the second-order kernels were not consistent with an LNL cascade model, since any significant smoothing before the first significant nonlinearity would produce a second-order kernel with interactions at nonzero relative lags, hence with a ridge not limited to the main diagonal. An NLN model was found to provide fits that were significantly better than the linear kernels alone. The relative dynamics of facilitation, inhibition, and linear response seen in the second-order kernels suggested that facilitation can be represented by a static, or zero-memory, nonlinearity and that the inhibition occurring after the center linear stage of the NLN model is delayed with respect to the linear response. These terms are represented in Eq. 8, which was fitted to the three second-order kernels (UV–UV, green–green, and UV–green) in order to quantify their differences. The %MSPEs for these models are given in Table I, and the parameter values obtained are summarized in Table III. In the case of the vertical stimulus we were able to improve the mean %MSPE of the nonlinear cells from 19.1% using a linear parametric model, to 15.8% using both linear and nonlinear terms for $n = 4$ cells. In the experimental setup where the horizontally mounted stimulus was used, the addition of second-order terms produced smaller residuals for $n = 29$ cells, reducing the mean %MSPE for these cells from 18.5% to 15.7%. Given that these models contain only 14 parameters, they represent a large gain in efficiency from the full second-order kernel models, which contain 2015 parameters, and had an average %MSPE of 12.9% for these sets of cells.

Effects of Temperature

In five of the six cells tested, temperature effects were sufficiently reversible for inclusion in the dataset (see MATERIALS AND METHODS). We found that in general, the linear and nonlinear receptor response became faster and larger, but that the effects on the relative contribution of nonlinear kernels, and on UV/green ratio were variable. The mean time to peak response was 8.5 ms (SD = 0.8, $n = 10$) at elevated temperatures (28°C–33°C) compared with 13.5 ms (SD = 1.1, $n = 10$) for the same cells at lower temperatures (22°C–24°C). Fig. 8 shows an example of the first- and second-order kernels for a cell at 22°C, where the peak response occurred at 12.8 ms, and at 33°C when it occurred at 8.0 ms. This cell shows an increase in both UV and green amplitudes. Three of five cells had similar increases in UV amplitude; increasing, on average, to 210% of their original value, however two cells had small decreases in the amplitudes of their linear UV response (decreased to 97% and 92% of their original values). Green response amplitudes increased in magnitude for four cells (mean increase to 267% of original value, SD = 264%) and decreased for one to 37% of its original value (as shown in Fig. 9).

The effect of temperature on the magnitude of the linear and nonlinear response was variable. Only one cell showed a larger amount of power in its linear UV kernel from 44.3%, at 22°C, to 84.4%, at 32°C. The relative power in the linear green kernels increased for four out of five cells (mean increase of 186%) and decreased for the remaining cell to 94% of its original value. Three out of five cells had a reduction in power of the total component of nonlinear response (mean reduction of 44% [SD = 16%]) at higher tempera-

tures. However, for two cells it was increased to 158% and 111% of the original value.

The relative changes in UV and green response were also not uniform: four cells decreased their UV/green ratio at elevated temperatures from a mean of 4.1 (SD = 0.5, $n = 5$) to a mean of 3.0 (SD = 0.8, $n = 5$), and one increased its UV/green ratio at elevated temperatures from 9.3 to 38.0. Fig. 8 shows an example of the first- and second-order kernels for a cell that reduced its UV/green ratio from 3.9 at 22°C to 2.2 at 33°C, and Fig. 9 shows the kernels for the cell that increased its UV/green ratio.

Parametric fits were made of the receptor kernels at higher temperatures in order to ascertain the effect of elevated temperature on the shape of response. Results of these fits for the cells at elevated temperatures together with the control values can be found in Tables II and III. The mean estimate of the parameter t_u^p, the time to peak of the underlying log-normal process decreased from 17.6 ms (SD = 1.5 ms) to 11.1 ms (SD = 1.0 ms). If the temperature change of each experiment was taken into account, this converted to a mean Q_{10} for t_u^p of 1.9 (SD = 0.3). A Q_{10} value of 2.4 (SD = 0.5) was found for τ_u^d and τ_g^d that decreased in mean value from 12.8 ms (SD = 3.7 ms) to 6.2 ms (SD = 1.1 ms).

Unlike the parameters v_u, v_g, t_u^p, t_g^p, τ_g^d, and τ_u^d, we found that σ_u and σ_g, which describe the relative width of the underlying log-normal processes, did not significantly change with an increase in temperature, nor did the parameters of the nonlinear model describing the interaction of UV with itself (a_1 and b_1) or between UV and green (b_2). However, the mean green–green facilitation (a_2) and green–green inhibition (b_3) were significantly increased at higher temperatures (Table III). The latency of the inhibition that was assumed to be the same for all inhibitory effects (τ_i) also markedly decreased from 5.0 ms to 2.0 ms, which resulted in a mean Q_{10} for τ_i of 3.1.

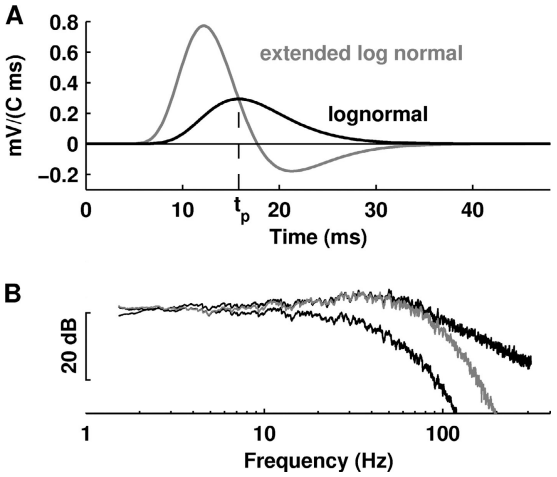

Figure 10. (A) A comparison of the log-normal and modified log-normal models with the same parameters values for (v_u, t_u^p, σ_u). The parameters were obtained by fitting the extended log-normal model (Eq. 6) to the first-order kernel of a receptor neuron. The peak response is larger and the time at which peak response actually occurs is earlier for the extended log-normal function. (B) Comparison of the response power spectra for the linear models seen in A: the extended log-normal model (middle line) and log-normal model with equivalent parameters (bottom line). The top line indicates the power spectrum of the recorded signal.

DISCUSSION

Spatial Resolution

The electrophysiologically determined values of $\Delta\rho = 15°$ in elevation and $\Delta\rho = 28°$ in azimuth are much smaller than the total field of view of the ocellus, of $120° \times 60°$, showing that the median ocellus of *H. tau* is not just a single sensor that can only detect intensity changes in time, but, rather, that it is capable of some resolution in space. However, the spatial resolution is at the low end when compared with electrophysiological data from other arthropod eyes, including simple eyes as well as compound eyes of both the apposition and superposition type (Warrant and McIntyre, 1993). Consequently, we need to consider the possibility that actual resolution is better and that the optics of the ocellus were degraded by the dissection procedure. This is unlikely. In earlier work (Stange et al., 2002), the spatial resolution of the median ocellus of *H. tau* was investigated by an entirely noninvasive ophthalmoscopic procedure, examining the angular extent of a patch of light (eyeshine) reflected from the fundus of the eye (tapetum), for illumination by a beam of parallel light. As the tapetum is located at the same distance from the lens as the bulk of the photopigment in the receptor neurons, this method provides a relevant estimate of angular sensitivity. Relative to the direction of incident light, a given eyeshine patch is visible over no more than 12° in elevation and 24° in azimuth, and the number of separate eyeshine patches that can be accommodated within the whole visual field is $\sim 5 \times 5$. Those values are consistent with the present observations.

The finding that the angular sensitivity functions are anisotropic, with an aspect ratio of 2, is also consistent with eyeshine measurements and is easily reconcilable with geometry of the ocellar lens (Stange et al., 2002). This is distinct from the situation in apposition compound eyes: although differences between horizontal and vertical interommatidial angles ($\Delta\varphi$) are not uncommon, differences for $\Delta\rho$ remain to be observed. There does not seem to be an optical way to achieve a deformed acceptance angle (Zeil et al., 1986).

Regarding the question as to what the underlying functional adaptation of this anisotropy might be, Stange et al. (2002) suggested that reduced acuity in az-

imuth constitutes a spatial low-pass filter that averages out unwanted information about local irregularities in horizontally extended features such as the skyline. They also suggested that a high acuity in elevation enables local intensity comparisons, allowing the detection of horizontal edges or even movements. As an alternative, we suggest that the adaptive feature consists of maximizing the field of view in azimuth, rather than maximizing resolution in elevation: the presence of a panoramic field of view could enable the ocellus to detect roll, because the rotation of the horizon associated with roll will lead to an imbalance of illumination from opposite sides.

Temporal Linear Response

Almost all cells (56/58) exhibited linear responses to both UV and green stimuli, and although the relative amplitudes varied from cell to cell, the UV and green temporal responses were indistinguishable. These receptors are therefore not capable of distinguishing between UV and green stimuli on the basis of their linear response alone. Since these components make up the largest component of the response of these cells it seems unlikely that the ocellar retina is capable of color discrimination.

Small signal or linear responses within the receptors of other invertebrate compound eyes have been found to be well described by the log-normal function: locusts, crickets, flies, mantids, blowflies, dragonflies (Howard et al., 1984), and *Drosophila* (Juusola and Hardie, 2001b). Here we find that the linear response of the dragonfly ocellar receptor has a form that contains a distinctive undershoot as the membrane potential returns to equilibrium (Fig. 5, A and C). The range of mean estimates for the time to peak of the underlying log-normal process for both UV and green receptor response was found to be 16.3–17.6 ms. This is comparable to that of the dragonfly compound eye receptors at comparable temperatures where it was estimated to be 17.5 ms (SD = 0.4) (Howard et al., 1984). Similarly, the range of widths (σ_x) of the underlying log-normal processes measured here was 0.275–0.297, which is comparable to that found in dragonfly compound eye receptors, where it was 0.277 (SD = 0.015) (Howard et al., 1984). Given the similarity in fundamental waveforms, it seems likely that the phototransduction machinery is conserved between dragonfly ocellar and compound eye receptors.

To account for the distinctive biphasic form of the temporal responses, we extended the log-normal model to include a component proportional to the derivative of the log-normal. Similar dynamics have been seen in receptor neurons of other insects (Juusola and Weckström, 1993; Matic, 1983; James and Osorio, 1996). In blowfly, the amplitude of the undershoot increases with the adapting background (Juusola and Weckström, 1993). Although we did not observe different undershoot amplitudes between the cells stimulated at different adapting levels, this was possibly because we did not modulate the background through a large enough range in this study. In butterflies the biphasic response of receptors is thought to occur as a result of electrically mediated inhibition between receptors with different spectral sensitivities (Matic, 1983). This is not the case for some of the cells in this study, which show the distinct phasic components even when they respond exclusively to UV stimulus.

We found that the amplitudes of the undershoot for both UV (τ_u^d) and green (τ_g^d) are temperature sensitive, in all cells decreasing with a $Q_{10} \sim 2$. The reduction in the contribution of this component means the linear response is smaller in amplitude and slower. These changes partially offset the effects of temperature on the underlying log-normal response, which is larger and faster.

The function of the extra phasic component in the dragonfly ocellar receptors could lie in the fact that its addition enhances the cellular response to high frequency signals (Fig. 10 B) and decreases the relative contribution of the tonic response, thus removing some of the redundant receptor signal that is correlated in time (van Hateren, 1997). Therefore, in the dragonfly ocellus, receptors appear to perform some early linear processing of the light signal, unlike other invertebrates where the tonic response of the receptors is removed during the transfer of the signal to the next cells in the visual pathway (van Hateren, 1997).

Underlying Linear Mechanisms

In our model of the linear response, we have used the derivative of the original log-normal signal to produce the phasic component (Fig. 10 A). It is not difficult to see how the cell could produce this derivative electrically. For example, the equation that describes the full linear response, Eq. 6, is analogous to the circuit equation that describes the voltage $G_u(t)$ across a capacitor (capacitance, C) in parallel with a resistor (resistance, R) and light-induced voltage supply, $H_u(t)$, in series. In that case, $\tau_u^d = RC$. This type of model could explain the observed shape of the linear impulse response and would be consistent with the observation that decreases in the time constants τ_u^d and τ_u^d with a $Q_{10} \sim 2$ are consistent with similar changes in the membrane time constant of previous studies (French and Järvilehto, 1978; Juusola and Hardie, 2001b).

Temporal Nonlinear Response

The differences in horizontal and vertical receptive fields (Figs. 2 and 3) mean that more light is integrated spatially by the receptor when the display is mounted

horizontally than vertically. This means that the cell observes greater mean intensities when the display was mounted horizontally and could explain why we found a greater number of "nonlinear" cells in this case. Increasing the stimulus contrast also increases the nonlinear component of the reconstructed receptor response but this effect is significantly reduced at lower mean light intensities.

The larger component of UV self-facilitation than green self-facilitation is not due to the system being driven by UV stimuli to a larger linear response, as the amplitude of linear temporal response (for stimulus type II) was similar in both horizontal and vertical experiments. This is also reflected in the parameter values representing the magnitudes of facilitation (a_1 and a_2). These are fitted taking into account the magnitude of the linear response and are therefore indicative of a cell's capacity to amplify signals regardless of their size. These parameters can be used to test the possibility that the smaller levels of self-facilitation seen in the green kernels than those seen in the UV kernels are a direct result of a smaller green linear response than the UV linear response. For almost all cells this is the not the case (Table III), as is shown in Fig. 7. Thus, the fact that the linear green response is smaller than the linear UV response does not account for UV self-facilitation being larger than green self-facilitation.

A possible function of the nonlinear responses seen in the receptor neurons seen here is to maintain a higher gain at higher frequencies. For example, the amplitude response of the nonlinear kernel model is able to maintain its amplitude response at higher frequencies than the linear model alone (Fig. 10 B). Nonlinear summation may also be used to discriminate between UV and green illumination if differential amplification of these responses occurs. While it is also possible that the inhibition observed between UV and green pathways could also be used for enhancing color discrimination (analogous to lateral inhibition enhancing spatial resolution), it seems more likely that any functionality of this process would be superseded by the fact that the linear responses of these cells to UV and green light, which dominate their response, are indistinguishable.

Temperature Effects

A change of temperature from 23°C to 31°C has several distinguishable effects on the responses. The temporal response to green and UV light becomes markedly faster and its amplitude increases. The decrease in the times to peak (t_u^p and t_g^p) and increase in amplitudes (v_u and v_g) without significant changes in width of the response waveform (σ_u and σ_g) are consistent with results from other insect sensory systems: in blowfly (*Calliphora vicina*) the Q_{10} for t_g^p, v_g, and σ_g have been estimated to be 0.67, 1.28, and 0.8, respectively (Tatler et al., 2000), and in *Drosophila* the Q_{10} for the time to peak has been estimated to be 2.5 (Juusola and Hardie, 2001b). Like other studies, we find that the width of the log-normal response is much less temperature sensitive than the time to peak.

The relative sensitivities to green and UV also change, albeit by different amounts and with different signs in different receptor neurons. This could indicate two different subpopulations of cells, as described in the dragonfly compound eye (Laughlin, 1976), or it could be the result of the pupil mechanism demonstrated in the median ocellus of other dragonflies (Stavenga et al., 1979, *Sympetrum* and *Anax junius*). In that case, the exposure of dark-adapted ocelli to light induced a UV-sensitive pigment to migrate over distinct pathways on the retina. Pigment migration has also been shown to be temperature induced (Nordström and Warrant, 2000). Cells that are screened by the pigment would be expected to have a reduced UV sensitivity compared with those that are not.

The lower limit for the ecologically relevant temperature range for *H. tau* is around 20°C (see also Corbet, 1999), and furthermore, dragonflies are capable of active temperature regulation. May (1995) measured body temperatures in *Anax junius* immediately after capturing flying animals from the field, at ambient temperatures between 21°C and 38°C, and found that head temperature was maintained above 30°C. Therefore, our measurements at the higher temperature are more representative of natural conditions, including the UV/green ratio.

Underlying Nonlinear Mechanisms

The light-induced current of receptor neurons has been found to be linear in most receptors of invertebrates. However, the light-induced response can be dynamically modulated by intracellular processes (Weckström et al., 1992) and by the electrical properties of its membrane (Juusola and Weckström, 1993; Laughlin, 1996). Furthermore, synaptic and electrical coupling between adjacent receptors and between receptors and second-order neurons may provide feedback mechanisms that modify the response properties of these cells (Klingman and Chappell, 1978; Laughlin, 1981; Stone and Chappell, 1981; Simmons, 1982).

A number of cellular mechanisms could underlie the self-facilitation of the UV and green response in the receptor neurons we studied. Juusola et al. (2003) found that *Shaker* K^+ channels contribute to a similar static nonlinearity. However, our results are not consistent with this type of mechanism since voltage-sensitive channels act to modulate the light-induced voltage changes and would therefore act downstream of the linear process. Only a fast acting process early in the

transduction process could explain the static facilitation seen here.

The fast reconversion of rhodopsin through the photoisomerization of metarhodopsin to rhodopsin is a possible candidate. This process occurs on a fast time scale in the order of 100 μs (Kirschfeld et al., 1971), which is consistent with our results. However, it is also thought to underlie paired-pulse inhibition between pulses of short (blue) and long (red) wavelength light (Hamdorf and Kirschfeld, 1980). We observed no fast static interactions (only delayed) of any kind between UV stimuli and green stimuli.

Another possibility is that the fast facilitation seen here is the result of a sensitizing pigment. Evidence from fly receptors indicates that the purported sensitizing pigment can transfer absorbed energy to both the rhodopsin and metarhodopsin molecules (Minke and Kirschfeld, 1979). Evidence from fly ocelli suggests the presence of a sensitizing pigment (Kirschfeld et al., 1988). While there is no similar data for dragonfly ocelli, a concurrent decrease in relative UV sensitivity with a decrease in temperature was found in *Calliphora* compound eye receptors (Järvilehto et al., 1984; Weckström et al., 1985), and suggested as evidence of the existence of a sensitizing pigment. In our case, four out of the five receptors that were tested showed the same behavior.

Inhibition in these receptor cells occurs after the transduction process. It could originate from a variety of sources including calcium inactivation of the light-induced current (Hardie and Minke, 1994), delayed rectifying K^+ channels (Juusola et al., 2003), synaptic feedback from other receptors or L-neurons (Laughlin, 1981), and electrically mediated lateral inhibition between cells (Shaw, 1975). Although we could not rule out the influence of any of these mechanisms, the last of these is unlikely to have the ∼4-ms delay we observed between peak linear response and peak inhibition. This delay would be consistent with synaptic feedback from the L-neurons, and evidence from electrode studies combined with pharmacological blockade indicates that this feedback is negative, consistent with the inhibition seen here (Stone and Chappell, 1981). The large decrease in the latency of the inhibition (τ_i) with temperature ($Q_{10} \sim 3.1$) is also consistent with the idea that synaptic feedback underlies the inhibition seen here, as results from another invertebrate (*Limulus*) have shown synaptic latency to be strongly temperature dependent ($Q_{10} \sim 5$; Adolph, 1973).

We thank Ted Maddess for his many useful suggestions.

This work was sponsored by the Air Force Office of Scientific Research (AFOSR/AOARD special contract 03-4009).

Olaf S. Andersen served as editor.

Submitted: 2 May 2005
Accepted: 27 September 2005

REFERENCES

Adolph, A.R. 1973. Thermal sensitivity of lateral inhibition in *Limulus* eye. *J. Gen. Physiol.* 62:392–406.

Anderson, J.C., and S.B. Laughlin. 2000. Photoreceptor performance and the coordination of achromatic and chromatic inputs in the fly visual system. *Vision Res.* 40:13–31.

Chappell, R.L., and R.D. DeVoe. 1975. Action spectra and chromatic mechanisms of cells in the median ocelli of dragonflies. *J. Gen. Physiol.* 65:399–419.

Chappell, R.L., and J.E. Dowling. 1972. Neural organization of the median ocellus of the dragonfly. I. Intracellular electrical activity. *J. Gen. Physiol.* 60:121–147.

Corbet, P.S. 1999. Dragonflies: behaviour and ecology of *Odonata*. Harley Books, Martins, Essex, UK. 829 pp.

Dowling, J.E., and R.L. Chappell. 1972. Neural organization of the median ocellus of the dragonfly. II. Synaptic structure. *J. Gen. Physiol.* 60:148–165.

French, A.S., and M. Järvilehto. 1978. The dynamic behaviour of photoreceptor cells in the fly in response to random (white noise) stimulation at a range of temperatures. *J. Physiol.* 274:311–322.

French, A.S., M.J. Korenberg, M. Järvilehto, E. Kouvalainen, M. Juusola, and M. Weckström. 1993. The dynamic nonlinear behaviour of fly photoreceptors evoked by a wide range of light intensities. *Biophys. J.* 65:832–839.

Hamdorf, K., and K. Kirschfeld. 1980. Reversible events in the transduction process of photoreceptors. *Nature.* 283:859–860.

Hardie, R.C., and B. Minke. 1994. Calcium-dependent inactivation of light-sensitive channels in *Drosophila* photoreceptors. *J. Gen. Physiol.* 103:409–427.

Howard, J., A. Dubs, and R. Payne. 1984. The dynamics of phototransduction in insects. A comparative study. *J. Comp. Physiol.* 154:159–182.

James, A.C. 2003. The pattern-pulse multifocal visual evoked potential. *Invest. Ophthalmol. Vis. Sci.* 44:879–890.

James, A.C., and D. Osorio. 1996. Characterization of columnar neurons and visual signal processing in the medulla of the locust optic lobe by system identification techniques. *J. Comp. Physiol.* 178:183–199.

James, A.C., R. Ruseckaite, and T. Maddess. 2005. Effect of temporal sparseness and dichoptic presentation on multifocal visual evoked potentials. *Vis. Neurosci.* 22:45–54.

Järvilehto, M., M. Weckström, and E. Kouvalainen. 1984. Spectral sensitivity in insect photoreceptors at a range of temperatures. *Acta. Physiol. Scand. Suppl.* 537:81–86.

Juusola, M., and G.G. de Polavieja. 2003. The rate of information transfer of naturalistic stimulation by graded potentials. *J. Gen. Physiol.* 122:191–206.

Juusola, M., and A.S. French. 1997. Visual acuity for moving objects in first- and second-order neurons of the compound eye. *J. Neurophysiol.* 77:1487–1495.

Juusola, M., and R. Hardie. 2001a. Light adaptation in *Drosophila* photoreceptors: I. Response dynamics and signaling efficiency at 25°C. *J. Gen. Physiol.* 117:3–25.

Juusola, M., and R. Hardie. 2001b. Light adaptation in *Drosophila* photoreceptors: II. Rising temperature increases the bandwidth of reliable signalling. *J. Gen. Physiol.* 117:27–41.

Juusola, M., and M. Weckström. 1993. Band-pass filtering by voltage-dependent membrane in an insect photoreceptor. *Neurosci. Lett.* 154:84–88.

Juusola, M., J.E. Niven, and A.S. French. 2003. Shaker K^+ channels contribute early nonlinear amplification to the light response in *Drosophila* photoreceptors. *J. Neurophysiol.* 90:2014–2021.

Kirschfeld, K., R. Feiler, and B Minke. 1971. The kinetics of formation of metarhodopsin in intact photoreceptors of the fly. *Kyber-*

netik. 9:159–182.

Kirschfeld, K., R. Feiler, and K. Vogt. 1988. Evidence for a sensitizing pigment in the ocellar photoreceptors of the fly (*Musca*, *Calliphora*). *J. Comp. Physiol.* 163:421–423.

Klingman, A., and R.L. Chappell. 1978. Feedback synaptic interaction in the dragonfly ocellar retina. *J. Gen. Physiol.* 71:157–175.

Laughlin, S.B. 1976. The sensitivities of dragonfly photoreceptors and the voltage gain of transduction. *J. Comp. Physiol.* 111:221–247.

Laughlin, S.B. 1981. Neural principles in the visual system. *In* Comparative Physiology and Evolution of Vision in Invertebrates: Handbook of Sensory Physiology. Vol. VII/6 B. H. Autrum, editor. Springer, New York. 135–280.

Laughlin, S.B. 1996. Matched filtering by a photoreceptor membrane. *Vision Res.* 36:1529–1541.

Lee, Y.W., and M. Schetzen. 1965. Measurement of Wiener kernels of a non-linear system by cross-correlation. *Int. J. Control.* 2:237–254.

Marmarelis, P.Z., and G.D. McCann. 1973. Development and application of white noise modeling techniques for studies of insect visual nervous system. *Kybernetik*. 12:74–89.

Matic, T. 1983. Electrical inhibition in the retina of the butterfly *Papilio*. I. Four spectral types of photoreceptors. *J. Comp. Physiol.* 152:169–182.

May, M. 1995. Simultaneous control of head and thoracic temperature by the green darner dragonfly *Anax junius* (*Odonata*: *Aeshnidae*). *J. Exp. Biol.* 198:2373–2384.

McCann, G.D. 1974. Nonlinear identification theory models for successive stages of visual nervous systems of flies. *J. Neurophysiol.* 37:869–895.

Minke, B., and K. Kirschfeld. 1979. The contribution of a sensitizing pigment to the photosensitivity spectra of fly rhodopsin and metarhodopsin. *J. Gen. Physiol.* 73:517–540.

Mizunami, M. 1995. Functional diversity of neural organisation in insect ocellar systems. *Vision Res.* 35:443–452.

Nordström, P., and E.J. Warrant. 2000. Temperature induced pupil movements in insect superposition eyes. *J. Exp. Biol.* 203:685–692.

Payne, R., and J. Howard. 1981. Response of an insect receptor: a log-normal model. *Nature.* 290:415–416.

Press, W.H., B.P. Flannery, S.A. Tuekolsky, and W.T. Vetterling. 1993. Numerical Recipes in C. The Art of Scientific Computing. Second ed. Cambridge University Press, Cambridge, UK. 994 pp.

Ruck, P. 1961. Electrophysiology of the insect dorsal ocellus. I. Origin of the components of the electroretinogram. *J. Gen. Physiol.* 44:605–627.

Ruck, P. 1965. The components of the visual system of a dragonfly. *J. Gen. Physiol.* 49:289–307.

Sakai, H.M., K.-I. Naka, and M. Korenberg. 1988. White-noise analysis in visual neuroscience. *Vis. Neurosci.* 1:287–296.

Shaw, S.R. 1975. Retinal resistance barriers and electrical lateral inhibition. *Nature.* 255:480–483.

Simmons, P.J. 1982. The operation of connexions between photoreceptors and large second-order neurones in dragonfly ocelli. *J. Comp. Physiol.* 149:389–398.

Stange, G., S. Stowe, J.S. Chahl, and A. Massro. 2002. Anisotropic imaging in the dragonfly median ocellus: a matched filter for horizon detection. *J. Comp. Physiol.* 188:455–467.

Stone, S.L., and R.L. Chappell. 1981. Synaptic feedback onto photoreceptors in the ocellar retina. *Brain Res.* 221:374–381.

Stavenga, D.G., G.D. Bernard, R.L. Chappell, and M. Wilson. 1979. Insect pupil mechanisms. III. On the pigment migration in dragonfly ocelli. *J. Comp. Physiol.* 129:199–205.

Tatler, B., D.C. O'Carroll, and S.B. Laughlin. 2000. Temperature and the temporal resolving power of fly photoreceptors. *J. Comp. Physiol.* 186:399–407.

van Hateren, J.H. 1997. Processing of natural time series of intensities by the visual system of a blowfly. *Vision Res.* 37:3407–3416.

Warrant, E., and P. McIntyre. 1993. Arthropod eye design and the physical limits to spatial resolving power. *Prog. Neurobiol.* 40:413–461.

Weckström, M., M. Järvilehto, E. Kouvalainen, and P. Järvilehto. 1985. Fly photoreceptors and temperature: relative UV-sensitivity is increased by cooling. *Eur. Biophys.* 12:173–179.

Weckström, M., M. Juusola, and S. Laughlin. 1992. Presynaptic enhancement of signal transients in photoreceptor terminals in the compound eye. *Proc. Roy. Soc.* 250:83–89.

Wong, F., B.W. Knight, and F.A. Dodge. 1980. Dispersion of latencies and the adapting-bump model in photoreceptors of *Limulus*. *J. Gen. Physiol.* 76:517–537.

Wilson, M. 1978. The functional organization of locust ocelli. *J. Comp. Physiol.* 124:297–316.

Yasui, S. 1979. Stochastic functional Fourier series, Volterra series, and nonlinear systems analysis. *IEEE Trans. Auto. Control.* 24:230–242.

Zeil, J., G. Nalbach, and H.-O. Nalbach. 1986. Eyes, eyestalks and the visual world of semi-terrestrial crabs. *J. Comp. Physiol.* 159: 801–811.